Segmenting France Across Four Centuries

Marta López-Rauhut[1,2], Hongyu Zhou[3,4], Mathieu Aubry[1], and Loic Landrieu[1]

[1] LIGM, ENPC, IP Paris, Univ Gustave Eiffel, CNRS, Marne-la-Vallée, France
[2] Université Paris-Saclay, CNRS, LISN, Orsay, France
[3] University of Bonn, Germany
[4] Lamarr Institute, Germany

Abstract. Historical maps offer an invaluable perspective into territory evolution across past centuries—long before satellite or remote sensing technologies existed. Deep learning methods have shown promising results in segmenting historical maps, but publicly available datasets typically focus on a single map type or period, require extensive and costly annotations, and are not suited for nationwide, long-term analyses.
In this paper, we introduce a new dataset of historical maps tailored for analyzing large-scale, long-term land use and land cover evolution with limited annotations. Spanning metropolitan France (548,305 km^2), our dataset contains three map collections from the 18th, 19th, and 20th centuries. We provide both comprehensive modern labels and 22,878 km^2 of manually annotated historical labels for the 18th and 19th century maps. Our dataset illustrates the complexity of the segmentation task, featuring stylistic inconsistencies, interpretive ambiguities, and significant landscape changes (e.g., marshlands disappearing in favor of forests).
We assess the difficulty of these challenges by benchmarking three approaches: a fully-supervised model trained with historical labels, and two weakly-supervised models that rely only on modern annotations. The latter either use the modern labels directly or first perform image-to-image translation to address the stylistic gap between historical and contemporary maps. Finally, we discuss how these methods can support long-term environment monitoring, offering insights into centuries of landscape transformation. Our official project repository is publicly available on GitHub.

Keywords: historical map segmentation · image-to-image translation

1 Introduction

Historical maps are invaluable for studying long-term changes in landscapes, infrastructure, and land use. By analyzing cartographic data spanning centuries, we can quantify transformations such as deforestation, urbanization, and the evolution of transportation networks. However, direct comparisons across historical maps are hindered by stylistic variations, inconsistencies in drawing conventions, and the lack of standardized annotations. This underscores the need for automatic methods capable of extracting meaningful semantic information from heterogeneous historical maps.
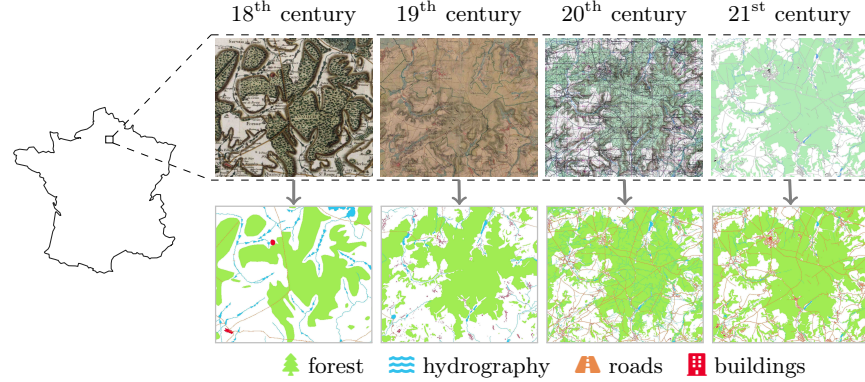
| 18th century | 19th century | 20th century | 21st century |

🌲 forest 〰 hydrography 🛣 roads 🏢 buildings

Fig. 1: **Semantic Segmentation of Historical Maps of France Spanning Four Centuries.** *Top row*: aligned input maps of the same area. The 21st-century map is a vectorized present-day map. *Bottom row*: semantic segmentation of each input map into four classes.

In this work, we introduce a large-scale dataset for historical map analysis, covering four centuries of cartography over metropolitan France, as shown in fig. 1. Our dataset provides historical map scans alongside modern land cover annotations and sparse historical annotations. This enables comparing supervised approaches, trained with historical labels, and weakly-supervised approaches, trained with modern labels.

To establish a benchmark for future research, we propose three baseline approaches. The first applies direct segmentation using sparse historical labels. The second employs a weakly-supervised framework, training a model to segment historical maps using modern land cover labels. The third incorporates a CycleGAN-based image-to-image translation module to translate historical maps into a modern cartographic style before segmentation, reducing stylistic discrepancies.

Our results highlight the strengths and limitations of these approaches, demonstrating their effectiveness in segmenting historical maps while illustrating the broader challenges of the task. We further show how our models can be leveraged to analyze long-term land cover changes across centuries at a national scale. By releasing this benchmark dataset and systematically evaluating multiple baselines, we provide a foundation for future research in automated historical map analysis, facilitating the study of environmental and urban transformations.

2   Related work

In this section, we review methods that have been applied to historical maps for semantic segmentation and image-to-image translation. In addition, we discuss how historical maps have been used to track and analyze long-term changes.

2.1   Semantic Segmentation of Historical Maps

While numerous studies address the segmentation of historical maps, most focus on isolating a single class or geographic feature: forests [25], railroads [9], bridges [70], roads [7,15,5], archaeological features [19], mines [44], cadastral parcels [3,2], wetlands [31,62,49], building footprints [23,24,35] or human settlements [64,65,66]. Here we focus on multi-class segmentation approaches and categorize them into two groups: traditional and deep-learning-based approaches.

Traditional Approaches. Early attempts at segmenting historical maps primarily relied on color-based segmentation [36,10], line extraction techniques [33], morphological operations [23], and watershed-based superpixels [46]. These methods do not require annotated training data but involve complex, multi-step pipelines that must be customized for each specific historical map. Additionally, they depend heavily on clear and consistent color-coding and well-defined boundaries between shapes.

Deep Learning Approaches. In recent years, deep learning has become the dominant approach for analyzing historical maps. While these methods reduce the need for manual engineering, they often require extensive annotated datasets, which can be costly to produce.

The majority of deep learning segmentation techniques that have been applied to historical maps are based on U-Net [54,44,19,7] or U-Net++ [75,15,42] architectures, which can be combined with Atrous Spatial Pyramid Pooling [71] or attention [5]. Some rely on other architectures such as region-based CNNs [55], simple FCNs [62] or Deeplabv3+ and Ma-Net [5]. Hybrid approaches, which combine deep learning with traditional techniques such as superpixels [46] or morphological operations [40], have also shown promise.

To address the scarcity of annotated data, several strategies have been proposed, including transfer learning [9,74], unsupervised domain adaptation [72], and weak supervision using contemporary [66,14,67] or multi-date [6] labels. Contemporary data can be leveraged more effectively by first homogenizing the visual style of historical and contemporary maps. This can be achieved through manual adaptation of symbology [32], overpainting historical maps with standard symbols [47], or using image-to-image translation methods, which we discuss in the next subsection.

Following these works, our baselines rely on a variation of the U-net architecture. We also include in our dataset modern labels adapted with a suitable level of detail and color scheme for each historical map.

2.2   Image-to-Image Translation on Maps

Image-to-image translation for geospatial data is often used to translate satellite images to maps rather than maps to maps. These approaches often rely on Cycle-GAN [76], but diffusion models have been used as well [63]. Recent approaches

improve the translated maps by leveraging color rendering information [37], external geographic data [73], cycle- and geometrical-consistency constraints [60], spatial attention [61], or a subset of closely-matched data [59].

Previous works have already experimented on the image-to-image translation of historical maps, mostly employing Pix2Pix [1], CycleGAN [38], or both [4,12], also in addition to CUT [70]. Some of them have focused on generating synthetic data to train text detection [38] or semantic segmentation [4,70] models.

We design a baseline based on CycleGAN, incorporating an additional translation loss accounting for weak annotations.

2.3   Tracking Centuries of Change

Historical maps are a valuable resource for understanding long-term dynamics in the social and natural sciences, especially when combined with aerial photography or remote sensing imagery [18]. Observing historical land use and land cover evolution trends can support the development of sustainable policies for landscape, ecosystem, and heritage conservation. Existing methods rely on segmentation through manual vectorization or labeling [56,53,52], multi-step color-based pipelines [23,68], object-based algorithms [39,69,16], or deep learning [42,45].

Although historical maps present unique challenges compared to remote sensing data [11], the extensive literature on change detection in geospatial data offers valuable insights. In particular, when detecting changes between datasets captured by heterogeneous sensors or formats, a significant challenge lies in distinguishing actual semantic changes from variations in appearance. This problem has been addressed by translating both images into a common representation using conditional adversarial networks [48] or autoencoders [21,41]. Our dataset and baselines emphasize how these challenges translate to historical maps.

3   Dataset

We propose a new multi-date dataset of historical maps of metropolitan France spanning four centuries. We provide full contemporary annotations, along with partial historical annotations, making it ideal for evaluating weakly- or semi-supervised learning approaches. As shown in tab. 1, our dataset exceeds comparable collections in both spatial and temporal coverage, while also offering more diverse annotations.

Composition. Our dataset covers 548,305 km^2 and is comprised of four aligned tile sets of 10,952 tiles, each tile being at least 1000×1000 pixels in size. These tile sets were sourced from four map collections, examples of which can be seen in fig. 1:

- **Cassini (18th c.).** Commissioned by Louis XIV, the Cassini maps charted the entire Kingdom of France from 1750 to 1815 using geodesic triangulation [50]. Their remarkable accuracy allows near-perfect alignment with modern maps.

Table 1: **Multi-Class Historical Map Datasets.** We report the characteristics of similar map collections. The column **Labels** indicates the percentage of the map surface that is densely annotated. **Classes** provides the nature of the labels, with possibly several subclasses per category. **Multi-date** refers to whether the dataset provides *aligned* maps of the same area belonging to different periods.

Dataset	Multi-date	Collection	Access	Location	Period	Scale	Extent in km²	Labels in %	Classes
Wu et al. [71]	✘	Siegfried	✉ ↺	CH	1880	1:25,000	23,048	100	≋
Martínez et al. [42]	✘	Cassini	✉	FR	1750-1815	1:86,400	10,000	100	🌲 ≋
Can et al. [7]	✘	Generalkarte	⬇	AT-HU	1884-1918	1:200,000	321,146	100	🛣
Ekim et al. [15]	✘	DHK Turkey	⬇	TR	1941-1943	1:200,000	132,970	100	🛣
Hosseini et al. [26]	✘	OS	⬇	GB	1888-1913	1:10,560	620	100	🏠 🚉
Paris [51]	∼	Maps of Paris	⬇	FR	1765-1994	≥1:2,000	≤105	100	🏠 ≋ 🛣
World [51]	∼	32 collections	⬇	90 countries	1720-1950	-	-	100	🏠 ≋ 🛣
Ours	✔	Cassini	⬇	FR	1750-1815	1:86,400	548,305	4.2	🌲 ≋ 🛣 🏠
		État-Major	⬇	FR	1820-1866	1:40,000	548,305	4.2	🌲 ≋ 🛣 🏠
		SCAN50	⬇	FR	1889-1922	1:50,000	548,305	0.0	🌲 ≋ 🛣 🏠
		Modern maps	⬇	FR	2019	Vectorized	548,305	100	🌲 ≋ 🛣 🏠

✔ *aligned* maps from multiple periods   ∼ *unaligned* maps from multiple periods   ✘ maps from a single period

✉ requires request   ↺ requires providers' authorization   ⬇ open-access + direct download

≋ hydrography   🌲 vegetation   🚉 rail   🛣 roads   🏠 buildings

– **Carte d'État-Major (19th c.).** Produced between 1820 and 1866 for the French military, these updates to the Cassini maps include topographic relief and individual buildings [27].
– **SCAN50 (20th c.).** Compiled in 1950 from map sheets produced during the first half of the 1900s, forming a cohesive mid-century map of France [28].
– **Modern maps (21st c.).** Contemporary multi-scale vector maps obtained from IGN, the French Mapping Agency.

IGN distributes these maps freely and in a common georeferenced coordinate system. We downloaded the historical maps at a scale of 1:40,000 and 150 DPI, corresponding to approximately 6.77 meters per pixel. We split the maps into sheets according to the Cassini mosaic. We selected the areas covered by all three historical maps, corresponding to 175 out of 181 sheets. In the rest of the paper, we refer to the four map collections as *Cassini, État-Major, SCAN50,* and *modern maps.*

Historical Labels. To evaluate our baselines, we selected 470 tiles (covering 22,878 km²) based on the extent of pre-existing annotations and terrain diversity. We obtained initial labels for Cassini from the GeoHistoricalData Project [20] and manually corrected them for registration issues, missing annotations, and minor errors using five labels: *forest, hydrography, roads, buildings,* and *background* (fig. 2). For État-Major, we completed partial labels provided by IGN. As no initial labels were available for SCAN50, we do not provide them. In total, the additional manual labeling process required approximately 160 hours.
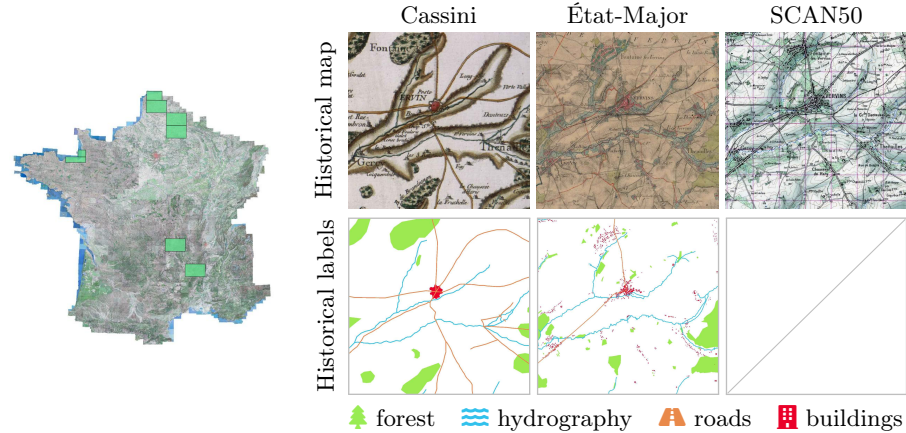
Fig. 2: **Historical Maps and Labels.** Our dataset covers three collections of historical maps. We provide manual annotations of the highlighted regions of France for the Cassini and État-Major collections.

4   Method

We introduce three baseline approaches for segmenting historical maps, illustrated in fig. 3. Our first approach is a fully-supervised model trained using scarce historical annotations (sec. 4.1). We also propose two weakly-supervised baselines that leverage abundant modern land cover labels (sec. 4.2). The first approach trains a segmentation model to directly map historical maps to modern land cover labels. The second approach first learns an image-to-image translation model to translate historical maps into a modern style, and then applies a segmentation model from modern maps to modern labels. All methods are evaluated on the same set of 470 tiles annotated for Cassini and État-Major.

4.1   Supervised Segmentation

This method leverages our manually annotated historical labels to train a model using a standard supervised approach. As it relies on historical annotations, this baseline can only be applied when significant annotation efforts can be made, but it can be expected to provide the best results.

   To evaluate this approach, we split the 470 annotated tiles into seven spatially distinct folds and perform 7-fold cross-validation. For each fold, we train a U-Net [54] using six folds and evaluate it on the held-out fold. The performance we report corresponds to the aggregation of the results on left-out folds. During training, we further divide the six folds into a training and validation set (80/20 split), using the validation set to select the best-performing epoch.
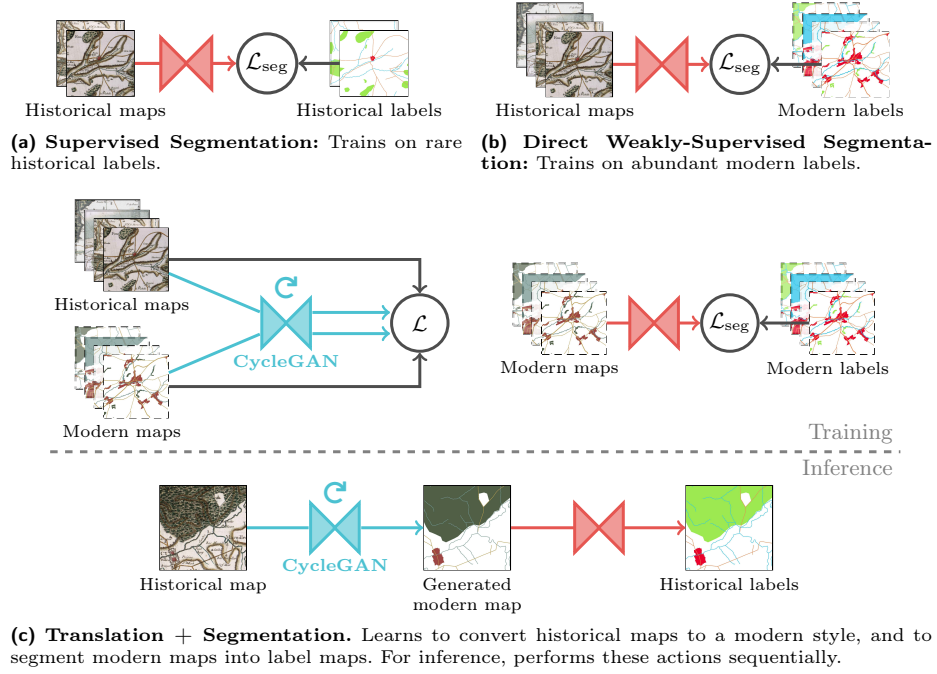
(a) **Supervised Segmentation:** Trains on rare historical labels.

(b) **Direct Weakly-Supervised Segmentation:** Trains on abundant modern labels.

(c) **Translation + Segmentation.** Learns to convert historical maps to a modern style, and to segment modern maps into label maps. For inference, performs these actions sequentially.

Fig. 3: **Historical Map Segmentation Baselines.** We train three semantic segmentation baselines to predict historical map labels, one supervised (fig. 3a) and two weakly-supervised (fig. 3b and fig. 3c).

4.2 Weakly-Supervised Segmentation

Manually annotating historical maps is labor-intensive, making it impractical for large-scale studies. In contrast, modern land cover labels can be freely obtained from open access vector-based GIS databases.

Direct Weakly-Supervised Segmentation. To leverage this, our first baseline is to train a U-Net to directly map historical maps to modern land cover labels. We exclude the 470 manually annotated tiles used for evaluation and split the remaining 10,482 historical tiles into 9,096 training tiles and 1,386 validation tiles. To obtain modern labels for each historical map, we select a level of detail consistent with its content, as visualized in the middle part of fig. 4.

Naturally, this task is highly challenging—asking the model, in essence, to "see" centuries into the future. However, we hypothesize that certain permanent landscape features, such as old-growth forests, major transportation corridors, and waterways, provide a supervisory signal, allowing the model to learn meaningful correspondences despite temporal discrepancies. However, training a segmentation model directly on weakly-aligned data becomes particularly chal-
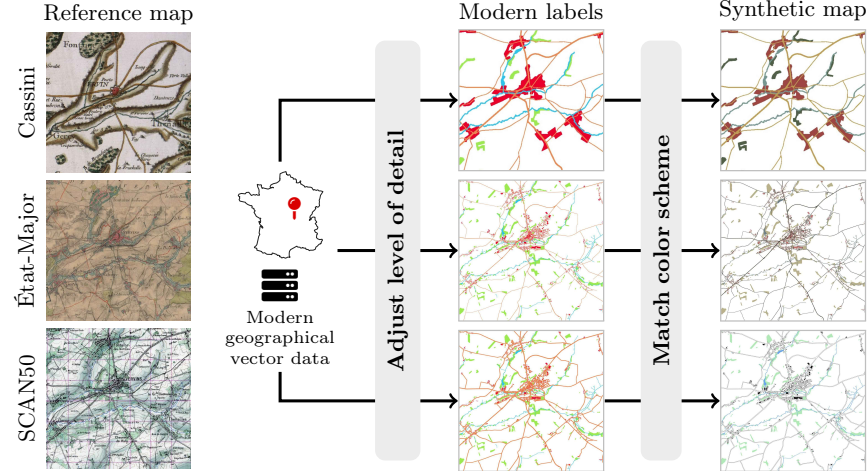
Fig. 4: **Modern Maps and Labels Workflow.** We tailor the level of detail and appearance of the modern vector map labels to each historical map collection, and then derive a synthetic modern map by colorizing the labels.

lenging when the temporal gap between historical maps and modern labels is large—for instance, in the case of Cassini maps, dating back to the 18th century.

Translation + Segmentation. To try and address this, our second weakly-supervised baseline follows a two-step pipeline:

- **Image-to-Image Translation.** We first train a model to translate historical maps into a modern cartographic style, reducing stylistic discrepancies while maintaining content consistency with the historical map, thanks to the cycle consistency loss.
- **Segmentation.** We then train a segmentation model on these translated maps to predict modern land cover labels.

To facilitate image-to-image translation, we generate synthetic modern maps by coloring modern label maps with a palette that mimics the appearance of historical maps, as visualized in the right part of fig. 4. This preprocessing step helps stabilize the translation training process.

For the image translation step, we employ a modified CycleGAN model, which we detail in the next section. Once translated, the historical maps adopt a visual style closer to modern maps, making them more compatible with segmentation models. Finally, we train a U-Net to segment these transformed maps into land cover labels.

4.3   Implementation Details

U-Net. We use an 8-stage nnU-Net [29] architecture modified to enable mirror padding. Each stage applies a 3×3 convolution with stride 2, except for the first

stage, which uses stride 1. Our training loop follows nnU-Net's default pipeline except we only use random resized crops as data augmentation. We train for 200 epochs with a batch size of 32. The cropping size is adjusted to match the scale of each historical map collection: 1000×1000 pixels for Cassini, and 500×500 pixels for État-Major and SCAN50.

CycleGAN. Given a source domain $\mathcal{X}$ and a target domain $\mathcal{Y}$, CycleGAN [76] learns an image translation function (or *generator*) $G_{\mathcal{X} \mapsto \mathcal{Y}} : \mathcal{X} \mapsto \mathcal{Y}$ that transforms images $x \in \mathcal{X}$ to the style of domain $\mathcal{Y}$. The introduction of a reverse mapping $G_{\mathcal{Y} \mapsto \mathcal{X}} : \mathcal{Y} \mapsto \mathcal{X}$ enables training on unaligned image pairs. Two domain *discriminators* $D_{\mathcal{X}}$ and $D_{\mathcal{Y}}$ distinguish between real and generated images. The total loss consists of three terms:

- The *adversarial loss* [22] $\mathcal{L}_{\mathrm{GAN}}$ encourages the generators to produce realistic outputs, and the discriminators to discriminate fake images from real ones.
- The *cycle consistency* loss $\mathcal{L}_{\mathrm{cyc}}$ ensures that translating an image to the opposite domain and back preserves its content.
- The *identity* loss $\mathcal{L}_{\mathrm{id}}$ regularizes the generators to maintain color consistency.

Barring temporal discrepancies and alignment errors, the content of historical and modern maps has some consistency. To leverage this weak alignment, we introduce an additional translation loss $\mathcal{L}_{\mathrm{tran}}$:

$$\mathcal{L}_{\mathrm{tran}} = \mathbb{E}_{x \sim \mathcal{X}} \| G_{\mathcal{Y} \mapsto \mathcal{X}}(y) - x \|_1 + \mathbb{E}_{y \sim \mathcal{Y}} \| G_{\mathcal{X} \mapsto \mathcal{Y}}(x) - y \|_1 \ . \tag{1}$$

The final objectives are:

$$\mathcal{L}(G_{\mathcal{X} \mapsto \mathcal{Y}}, G_{\mathcal{Y} \mapsto \mathcal{X}}) = \mathcal{L}_{\mathrm{GAN}} + \lambda_{\mathrm{cyc}} \mathcal{L}_{\mathrm{cyc}} + \lambda_{\mathrm{id}} \mathcal{L}_{\mathrm{id}} + \lambda_{\mathrm{tran}} \mathcal{L}_{\mathrm{tran}}, \tag{2}$$

$$\mathcal{L}(D_{\mathcal{X}}, D_{\mathcal{Y}}) = -\mathcal{L}_{\mathrm{GAN}}, \tag{3}$$

with λ_{cyc}, λ_{id} and λ_{tran} non-negative hyperparameters. We set $\lambda_{\mathrm{cyc}} = 1.0$, $\lambda_{\mathrm{id}} = 0.5$ and $\lambda_{\mathrm{tran}} = 0.5$ throughout all experiments.

We use ResNet-based generators with 9 blocks, while the discriminators are PatchGANs [30]. We train the networks for 100 epochs with a batch size of 1, a constant learning rate of 2×10^{-4} and apply the same random cropping and resizing strategy as for U-Net segmentation. Opposite to CycleGAN, which uses an image buffer to stabilize training by sampling fakes from previous iterations, we only consider fakes generated from the images in each batch, taking further advantage of the weak alignment.

5   Experiments

In this section, we first present our metrics and evaluation setting, then discuss qualitative and quantitative results, and finally present an application to long-term forest monitoring.

Table 2: **Quantitative Semantic Segmentation Results.** Overall Accuracy (OA) and dilated Intersection over Union (dIoU) for our three baselines and the two maps with available historical annotations.

Map	Baseline	OA	Mean dIoU	Per-class dIoU			
				🌲	🏢	〰	🛣
Cassini	Supervised	96.7	76.4	88.3	69.8	85.0	62.6
	Direct weakly-supervised	79.8	26.1	35.8	**5.3**	63.1	0.0
	Translation + segmentation	**85.3**	**36.1**	**56.1**	4.7	**70.9**	**12.7**
État-Major	Supervised	91.3	61.2	77.4	56.3	65.4	46.0
	Direct weakly-supervised	**83.3**	**38.6**	**49.6**	**39.6**	**58.6**	**6.3**
	Translation + segmentation	78.4	28.7	43.0	15.6	51.0	5.3

5.1   Evaluation and Metrics

We assess the baselines presented in sec. 4 using the 470 tiles annotated for the Cassini and État-Major maps. The evaluation is based on two metrics:

Overall Accuracy. This metric measures the proportion of correctly classified pixels across the entire test set. While this value provides a general assessment of segmentation quality, it can be biased by dominant classes, such as background pixels, and does not necessarily reflect performance on target classes.

Dilated IoU. This metric modifies the standard Intersection over Union (IoU) to account for slight misalignments between the prediction and the ground truth. Otherwise, small shifts disproportionally impact the precision measured for thin structures like roads and rivers. Standard IoU for a given class k is defined as:

$$\text{IoU}_k(P_k, T_k) = \frac{|P_k \cap T_k|}{|P_k \cup T_k|} \ , \tag{4}$$

where T_k (respectively, P_k) denotes the set of pixels labeled (respectively, predicted) as class k, and $|\cdot|$ denotes the size of a set. We add a tolerance to small misalignments by applying a dilation operator [58] that we write as Dil, which expands a set of pixels by a margin w in all directions. The dilated IoU (dIoU) [8] is then computed as:

$$\text{dIoU}_k(P_k, T_k) = \frac{|(\text{Dil}(P_k) \cap T_k) \cup (P_k \cap \text{Dil}(T_k))|}{|P_k \cup T_k|} \ . \tag{5}$$

For all experiments, we use $w = 3$ pixels. When computing the classwise average of dIoUs, we exclude the background class.
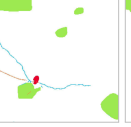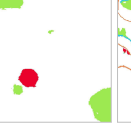
Fig. 5: **Qualitative Semantic Segmentation Results.** Predicted segmentation of our three baselines and SAM [34], on the same area across three centuries.

Evaluation Setting. To segment large tiles, we split them into patches of the same size used during training, without overlaps. As the performance of our translation + segmentation approach varies more across training runs than for the other models, we report the average of three models trained independently. The standard deviation for OA and mean dIoU is below 1.3 for Cassini, and 4.3 for État-Major.

5.2   Results and Analysis

We report quantitative and qualitative results for the semantic segmentation performance, a qualitative analysis of the image-to-image translation module and an ablation study.

Semantic Segmentation. We report in tab. 2 the performance of our baselines on the Cassini and État-Major maps, and illustrate their predictions in fig. 5. As expected, the fully-supervised method yields the best performance.

On the Cassini map, the translation + segmentation baseline consistently outperforms the other weakly-supervised approach, with forests, rivers, and roads all showing better recall. However, the relief lines of the Cassini maps are often misinterpreted as roads, causing lower precision, and the model also hallucinates roads and buildings. This behavior is unsurprising given that it is trained on modern labels, where roads and urban areas are more prevalent.

For the État-Major maps, direct weakly-supervised segmentation exhibits higher numerical performance, but qualitatively the translation + segmentation baseline delineates individual buildings, forest boundaries, roads, and rivers more

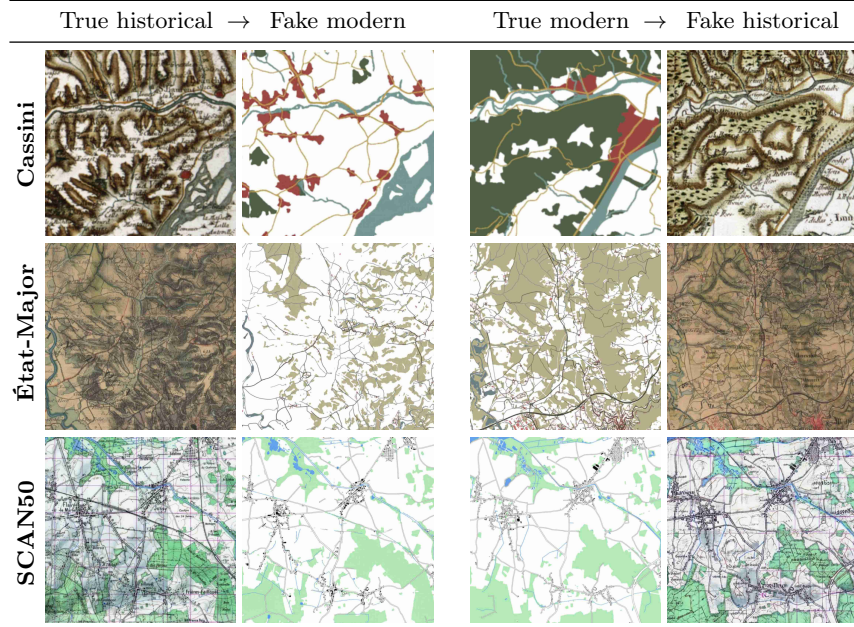| True historical → Fake modern	True modern → Fake historical

Fig. 6: **Image-to-Image Translation.** Examples of historical-to-modern and modern-to-historical generation with our image translation model (sec. 4.3).

accurately. Because the annotations for these maps only include main roads, predicting secondary roads is penalized even when they are correct.

Our analysis of the SCAN50 map is purely qualitative, as we do not have access to historical labels. Yet the results appear of high quality, likely because the smaller time gap between SCAN50 and modern reference data makes the modern labels more relevant. The translation + segmentation approach also produces more granular predictions for SCAN50, even detecting individual buildings.

Additionally, we illustrate in fig. 5 the segmentation predicted by the foundation model SAM [34] in a zero-shot setting. On the Cassini map, SAM accurately delineates forests and towns but fails to retrieve roads and rivers. Its predictions on the État-Major and SCAN50 maps are significantly worse. This suggests that the model, trained on natural images, struggles to generalize to historical maps, whose cartographic styles differ significantly from the data it was trained on.

In summary, our translation + segmentation baseline is arguably the most promising weakly-supervised approach. We thus analyze it further in the next paragraphs.

Qualitative Image-to-Image Translation Analysis. In fig. 6, we illustrate examples of image-to-image translation for all datasets in both directions: historical-to-modern and modern-to-historical. The generated historical

Table 3: **Quantitative Ablation Study.** Impact of the color and level of detail matching of the modern maps ("Match", see fig. 4), and the translation loss ($\mathcal{L}_{\text{tran}}$) on segmentation quality for our translation + segmentation baseline.

Map	Version		OA	Mean dIoU	Per-class dIoU			
	Match	$\mathcal{L}_{\text{tran}}$			🌲	🏢	〰	🚧
Cassini	✗	✗	61.7	17.6	22.2	4.7	29.8	13.6
	✓	✗	67.9	20.2	31.4	3.4	32.4	**13.6**
	✗	✓	83.8	31.8	46.4	**10.8**	57.6	12.5
	✓	✓	**85.3**	**36.1**	**56.1**	4.7	**70.9**	12.7
État-Major	✗	✗	51.6	10.6	22.2	8.8	9.8	1.6
	✓	✗	62.2	11.6	23.1	12.8	5.7	4.9
	✗	✓	**79.6**	**30.4**	**51.7**	**22.5**	44.8	2.5
	✓	✓	78.4	28.7	43.0	15.6	**51.0**	**5.3**

and modern maps appear visually credible, capturing the characteristic stylistic elements of their target domain, such as shading and color schemes. For SCAN50, the content is generally accurately translated, but this is not the case for Cassini and État-Major. We believe this is mainly due to the strong differences in the represented features and the strong distribution shift in classes. For example, most marshes from the 18th century have disappeared, while road networks and urban areas have greatly expanded, leading to frequent hallucinations in the generated maps.

Ablation Study. We assess the impact of two factors on our translation + segmentation baseline: (i) the color and level of detail adaptation of the synthetic modern maps to each historical map (fig. 4), and (ii) the addition of the translation loss $\mathcal{L}_{\text{tran}}$ (sec. 4.3). The corresponding quantitative and qualitative segmentation results are collected in tab. 3 and fig. 7 respectively. In general, qualitative results highlight the benefits of combining data adaptation with the translation loss on all datasets.

More in detail, data adaptation consistently helps on the Cassini maps except for building segmentation. On État-Major, adapting color and detail improves hydrography and roads but degrades other classes. The increased level of detail allows the model to segment thinner roads and smaller towns, but also introduces more false positives. Incorporating a translation loss improves the forest and hydrography segmentation for Cassini and État-Major, with tab. 3 showing a notable increase in dIoU and fig. 7 highlighting the improved forest precision for these two maps. For SCAN50, the impact of the translation loss is more limited as data adaptation appears sufficient to bridge the style gap.

5.3   Application: Long-Term Forest Monitoring

We evaluate the potential of our approach for long-term forest monitoring by tracking changes in predicted forest cover across metropolitan France from the

	Input	Match ✘ $\mathcal{L}_{\text{tran}}$ ✘	Match ✔ $\mathcal{L}_{\text{tran}}$ ✘	Match ✘ $\mathcal{L}_{\text{tran}}$ ✔	Match ✔ $\mathcal{L}_{\text{tran}}$ ✔	**Ground Truth**
Cassini						
État-Major						
SCAN50						

Fig. 7: **Qualitative Ablation Study.** Impact of color and level of detail matching of the modern maps ("Match", see fig. 4), and translation loss ($\mathcal{L}_{\text{tran}}$) on segmentation quality for our translation + segmentation baseline.

18$^{\text{th}}$ century to the present day. For each baseline and map collection, we use the predicted forest pixels to compute density maps and plot the results in fig. 8. Since the supervised baseline achieves the highest scores in tab. 2, its predictions can be regarded as the most reliable estimate of historical forest extent.

While the translation + segmentation baseline appears more precise than the direct weakly-supervised segmentation baseline in our experiments, it still over-predicts forest in the Landes region (◯) and mountainous areas (◯, ◯, ◯). This comes from often confusing marshes and relief shading with tree cover—an effect of relying on modern labels, where forests are more abundant.

Despite these caveats, our approach enables the reconstruction of three centuries of forest cover evolution across metropolitan France. Using the most reliable models (supervised baseline for the Cassini and État-Major collections, and translation + segmentation baseline for SCAN50), we identify trends that broadly align with historical records.

An Historical Perspective. From the Cassini maps, we see particularly dense woodlands in the northeast during the 18$^{\text{th}}$ century, which agrees with historical accounts of valuable forests in Franche-Comté [43]. Overall, forest cover has steadily increased over the last centuries, paralleling the rise of conservation policies in the 19$^{\text{th}}$ century—most notably, the founding of the first French National School of Forestry in Nancy in 1824, the Forestry Code of 1827, and subsequent reforestation laws in 1860 and 1882 targeting the Massif Central, the Pyrenees and the Alps [57]. Improved farmland productivity and the shift from wood to fossil fuels accelerated this trend [13]. In the southwest, we observe a marked

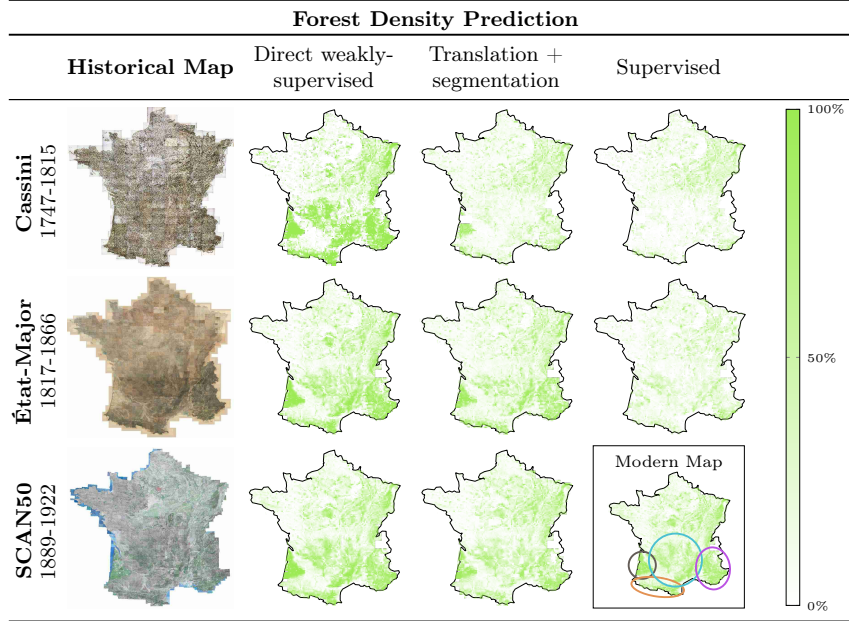| Forest Density Prediction			
Historical Map	Direct weakly-supervised	Translation + segmentation	Supervised

Fig. 8: **Predicted Forest Cover over France Across Four Centuries.** The framed map at the bottom right is the current forest density derived from contemporary sources. The colored ovals highlight key areas in our analysis: the Landes ⬭, Pyrenees ⬭, Massif Central ⬭, and Provence-Alps region ⬭.

increase in forested areas, reflecting the long-term transformation of marshlands in the Landes region from the 18$^{\text{th}}$ to the 20$^{\text{th}}$ centuries [17].

6   Conclusion

In this paper, we introduced a dataset for historical map segmentation that spans four centuries of metropolitan France. Our dataset provides extensive contemporary annotations as well as partial historical labels, enabling the evaluation of both fully- and weakly-supervised approaches. In particular, we demonstrated that translating historical maps into a modern style prior to applying a model trained solely on modern maps can significantly enhance segmentation performance. This highlights the promises of using modern labels to learn segmentation of unlabeled maps and enable long-term monitoring of landscape features, such as forests, across centuries. Furthermore, we outlined how these methods can be compared with other historical sources of information.

Since historical maps offer many crucial insights into a territory's past and its future trajectory, we hope our contributions will inspire further research into historical map segmentation with weak annotations. By mitigating the high cost

of manual labeling, such methods could advance large-scale, long-term studies of landscape change based on machine learning approaches.

7   Acknowledgments

References

1. Andrade, H.J.A., Fernandes, B.J.T.: Synthesis of satellite-like urban images from historical maps using conditional GAN. IEEE Geoscience and Remote Sensing Letters **19**, 1–4 (2022)
2. Ares Oliveira, S., Di Lenardo, I., Tourenc, B., Kaplan, F.: A deep learning approach to cadastral computing. In: Digital Humanities Conference (2019)
3. Ares Oliveira, S., di Lenardo, I., Kaplan, F.: Machine vision algorithms on cadaster plans. In: Premiere Annual Conference of the International Alliance of Digital Humanities Organizations (2017)
4. Arzoumanidis, L., Fethers, J.O., Mudiyanselage, S.H., Dehbi, Y.: Deep generation of synthetic training data for the automated extraction of semantic knowledge from historical maps. Abstracts of the ICA **7**, 7 (2024)
5. Avcı, C., Sertel, E., Kabadayı, M.E.: Deep learning-based road extraction from historical maps. IEEE Geoscience and Remote Sensing Letters **19**, 1–5 (2022)
6. Briand, S., Weissgerber, F., Fournier, P., Weissgerber, M.: LULC segmentation in historical images under domain shift: An empirical study. In: IGARSS 2024-2024 IEEE International Geoscience and Remote Sensing Symposium. pp. 488–492 (2024)
7. Can, Y.S., Gerrits, P.J., Kabadayi, M.E.: Automatic detection of road types from the third military mapping survey of Austria-Hungary historical map series with deep convolutional neural networks. IEEE Access **9**, 62847–62856 (2021)
8. Cheng, B., Girshick, R., Dollár, P., Berg, A.C., Kirillov, A.: Boundary IoU: Improving object-centric image segmentation evaluation. In: Proceedings of the IEEE/CVF Conference on Computer Vision and Pattern Recognition. pp. 15334–15342 (2021)
9. Chiang, Y.Y., Duan, W., Leyk, S., Uhl, J.H., Knoblock, C.A.: Training Deep Learning Models for Geographic Feature Recognition from Historical Maps, pp. 65–98. Springer (2020)
10. Chiang, Y.Y., Leyk, S., Knoblock, C.A.: Efficient and robust graphics recognition from historical maps. In: Graphics Recognition. New Trends and Challenges. pp. 25–35 (2013)
11. Chiang, Y.Y., Leyk, S., Knoblock, C.A.: A survey of digital map processing techniques. ACM Computing Surveys **47**(1), 1–44 (2014)

12. Christophe, S., Mermet, S., Laurent, M., Touya, G.: Neural map style transfer exploration with GANs. International Journal of Cartography **8**(1), 18–36 (2022)
13. Cinotti, B.: Evolution des surfaces boisées en France: Proposition de reconstitution depuis le début du XIXe siècle. Revue forestière française **48**(6), 547–562 (1996)
14. Duan, W., Chiang, Y.Y., Leyk, S., Uhl, J.H., Knoblock, C.A.: Automatic alignment of contemporary vector data and georeferenced historical maps using reinforcement learning. International Journal of Geographical Information Science **34**(4), 824–849 (2020)
15. Ekim, B., Sertel, E., Kabadayı, M.E.: Automatic road extraction from historical maps using deep learning techniques: A regional case study of Turkey in a German World War II map. ISPRS International Journal of Geo-Information **10**(8), 492 (2021)
16. Ettehadi Osgouei, P., Sertel, E., Kabadayı, M.E.: Integrated usage of historical geospatial data and modern satellite images reveal long-term land use/cover changes in Bursa/Turkey, 1858–2020. Scientific Reports **12**(1), 9077 (2022)
17. Ford, C.: The environmental transformation of "empty space": From desert to forest in the Landes of southwestern France. Comparative Studies in Society and History **65**(2), 422–445 (2023)
18. Fuchs, R., Verburg, P.H., Clevers, J.G., Herold, M.: The potential of old maps and encyclopaedias for reconstructing historic European land cover/use change. Applied Geography **59**, 43–55 (2015)
19. Garcia-Molsosa, A., Orengo, H.A., Lawrence, D., Philip, G., Hopper, K., Petrie, C.A.: Potential of deep learning segmentation for the extraction of archaeological features from historical map series. Archaeological Prospection **28**(2), 187–199 (2021)
20. GeoHistoricalData Project: GeoHistoricalData project website. `https://geohistoricaldata.org`, accessed: 2024-11-4
21. Gong, M., Niu, X., Zhan, T., Zhang, M.: A coupling translation network for change detection in heterogeneous images. International Journal of Remote Sensing **40**(9), 3647–3672 (2019)
22. Goodfellow, I., Pouget-Abadie, J., Mirza, M., Xu, B., Warde-Farley, D., Ozair, S., Courville, A., Bengio, Y.: Generative adversarial networks. Communications of the ACM **63**(11), 139–144 (2020)
23. Hecht, R., Herold, H., Behnisch, M., Jehling, M.: Mapping long-term dynamics of population and dwellings based on a multi-temporal analysis of urban morphologies. ISPRS International Journal of Geo-Information **8**(1), 2 (2018)
24. Heitzler, M., Hurni, L.: Cartographic reconstruction of building footprints from historical maps: A study on the Swiss Siegfried map. Transactions in GIS **24**(2), 442–461 (2020)
25. Herrault, P.A., Sheeren, D., Fauvel, M., Paegelow, M.: Automatic extraction of forests from historical maps based on unsupervised classification in the CIELab color space. Geographic Information Science at the Heart of Europe pp. 95–112 (2013)
26. Hosseini, K., Wilson, D.C., Beelen, K., McDonough, K.: MapReader: A computer vision pipeline for the semantic exploration of maps at scale. In: Proceedings of the 6th ACM SIGSPATIAL International Workshop on Geospatial Humanities. pp. 8–19 (2022)
27. Huguenin, M.: Historique de la cartographie de la nouvelle carte de France. IGN (1948)
28. IGN: SCAN Historique. `https://geoservices.ign.fr/scanhisto`, accessed: 2025-3-4

29. Isensee, F., Jaeger, P.F., Kohl, S.A., Petersen, J., Maier-Hein, K.H.: nnU-Net: A self-configuring method for deep learning-based biomedical image segmentation. Nature Methods **18**(2), 203–211 (2021)
30. Isola, P., Zhu, J.Y., Zhou, T., Efros, A.A.: Image-to-image translation with conditional adversarial networks. In: Proceedings of the IEEE Conference on Computer Vision and Pattern Recognition. pp. 1125–1134 (2017)
31. Jiao, C., Heitzler, M., Hurni, L.: Extracting wetlands from Swiss historical maps with convolutional neural networks. In: Proceedings of Automatic Vectorisation of Historical Maps. pp. 33–38 (2020)
32. Jiao, C., Heitzler, M., Hurni, L.: A fast and effective deep learning approach for road extraction from historical maps by automatically generating training data with symbol reconstruction. International Journal of Applied Earth Observation and Geoinformation **113**, 102980 (2022)
33. Khotanzad, A., Zink, E.: Contour line and geographic feature extraction from USGS color topographical paper maps. IEEE Transactions on Pattern Analysis and Machine Intelligence **25**(1), 18–31 (2003)
34. Kirillov, A., Mintun, E., Ravi, N., Mao, H., Rolland, C., Gustafson, L., Xiao, T., Whitehead, S., Berg, A.C., Lo, W.Y., et al.: Segment anything. In: Proceedings of the IEEE/CVF International Conference on Computer Vision. pp. 4015–4026 (2023)
35. Laycock, S.D., Brown, P.G., Laycock, R.G., Day, A.M.: Aligning archive maps and extracting footprints for analysis of historic urban environments. Computers & Graphics **35**(2), 242–249 (2011)
36. Leyk, S.: Segmentation of colour layers in historical maps based on hierarchical colour sampling. In: Graphics Recognition. Achievements, Challenges, and Evolution. pp. 231–241 (2010)
37. Li, J., Chen, Z., Zhao, X., Shao, L.: MapGAN: An intelligent generation model for network tile maps. Sensors **20**(11), 3119 (2020)
38. Li, Z., Guan, R., Yu, Q., Chiang, Y.Y., Knoblock, C.A.: Synthetic map generation to provide unlimited training data for historical map text detection. In: Proceedings of the 4th ACM SIGSPATIAL International Workshop on AI for Geographic Knowledge Discovery. p. 17–26 (2021)
39. Liu, D., Toman, E., Fuller, Z., Chen, G., Londo, A., Zhang, X., Zhao, K.: Integration of historical map and aerial imagery to characterize long-term land-use change and landscape dynamics: An object-based analysis via random forests. Ecological Indicators **95**, 595–605 (2018)
40. Liu, T., Miao, Q., Xu, P., Zhang, S.: Superpixel-based shallow convolutional neural network (SSCNN) for scanned topographic map segmentation. Remote Sensing **12**(20), 3421 (2020)
41. Luppino, L.T., Kampffmeyer, M., Bianchi, F.M., Moser, G., Serpico, S.B., Jenssen, R., Anfinsen, S.N.: Deep image translation with an affinity-based change prior for unsupervised multimodal change detection. IEEE Transactions on Geoscience and Remote Sensing **60**, 1–22 (2021)
42. Martinez, T., Hammoumi, A., Ducret, G., Moreaud, M., Deschamps, R., Piegay, H., Berger, J.F.: Deep learning ancient map segmentation to assess historical landscape changes. Journal of Maps **19**(1), 2225071 (2023)
43. Matteson, K.: Forests in revolutionary France: Conservation, community, and conflict, 1669–1848. Cambridge University Press (2015)
44. Maxwell, A.E., Bester, M.S., Guillen, L.A., Ramezan, C.A., Carpinello, D.J., Fan, Y., Hartley, F.M., Maynard, S.M., Pyron, J.L.: Semantic segmentation deep learn-

ing for extracting surface mine extents from historic topographic maps. Remote Sensing **12**(24), 4145 (2020)

45. Mäyrä, J., Kivinen, S., Keski-Saari, S., Poikolainen, L., Kumpula, T.: Utilizing historical maps in identification of long-term land use and land cover changes. Ambio **52**(11), 1777–1792 (2023)

46. Miao, Q., Liu, T., Song, J., Gong, M., Yang, Y.: Guided superpixel method for topographic map processing. IEEE Transactions on Geoscience and Remote Sensing **54**(11), 6265–6279 (2016)

47. Mühlematter, D.J., Schweizer, S., Jiao, C., Xia, X., Heitzler, M., Hurni, L.: Probabilistic road classification in historical maps using synthetic data and deep learning (2024), arXiv:2410.02250

48. Niu, X., Gong, M., Zhan, T., Yang, Y.: A conditional adversarial network for change detection in heterogeneous images. IEEE Geoscience and Remote Sensing Letters **16**(1), 45–49 (2018)

49. O'Hara, R., Marwaha, R., Zimmerman, J., Saunders, M., Green, S.: Unleashing the power of old maps: Extracting symbology from nineteenth century maps using convolutional neural networks to quantify modern land use on historic wetlands. Ecological Indicators **158**, 111363 (2024)

50. Perret, J., Gribaudi, M., Barthelemy, M.: Roads and cities of 18th century France. Scientific Data **2**(1), 1–7 (2015)

51. Petitpierre, R.G., Kaplan, F., Di Lenardo, I.: Generic semantic segmentation of historical maps. In: CEUR Workshop Proceedings. pp. 228–248 (2021)

52. Picuno, P., Cillis, G., Statuto, D.: Investigating the time evolution of a rural landscape: How historical maps may provide environmental information when processed using a GIS. Ecological Engineering **139**, 105580 (2019)

53. Pindozzi, S., Cervelli, E., Capolupo, A., Okello, C., Boccia, L.: Using historical maps to analyze two hundred years of land cover changes: Case study of Sorrento peninsula (south Italy). Cartography and Geographic Information Science **43**(3), 250–265 (2016)

54. Ronneberger, O., Fischer, P., Brox, T.: U-net: Convolutional networks for biomedical image segmentation. In: Medical Image Computing and Computer-Assisted Intervention. pp. 234–241 (2015)

55. Saeedimoghaddam, M., Stepinski, T.F.: Automatic extraction of road intersection points from USGS historical map series using deep convolutional neural networks. International Journal of Geographical Information Science **34**(5), 947–968 (2020)

56. San-Antonio-Gómez, C., Velilla, C., Manzano-Agugliaro, F.: Urban and landscape changes through historical maps: The Real Sitio of Aranjuez (1775–2005), a case study. Computers, Environment and Urban Systems **44**, 47–58 (2014)

57. Scheifley, W.H.: The depleted forests of France. The North American Review **212**(778), 378–386 (1920)

58. Serra, J.: Image analysis and mathematical morphology (1983)

59. Song, J., Chen, H., Du, C., Li, J.: Semi-MapGen: Translation of remote sensing image into map via semisupervised adversarial learning. IEEE Transactions on Geoscience and Remote Sensing **61**, 1–19 (2023)

60. Song, J., Li, J., Chen, H., Wu, J.: MapGen-GAN: A fast translator for remote sensing image to map via unsupervised adversarial learning. IEEE Journal of Selected Topics in Applied Earth Observations and Remote Sensing **14**, 2341–2357 (2021)

61. Song, J., Li, J., Chen, H., Wu, J.: RSMT: A remote sensing image-to-map translation model via adversarial deep transfer learning. Remote Sensing **14**(4), 919 (2022)

62. Ståhl, N., Weimann, L.: Identifying wetland areas in historical maps using deep convolutional neural networks. Ecological Informatics **68**, 101557 (2022)
63. Tian, J., Wu, J., Chen, H., Ma, M.: MapGen-Diff: An end-to-end remote sensing image to map generator via denoising diffusion bridge model. Remote Sensing **16**(19), 3716 (2024)
64. Uhl, J.H., Leyk, S., Chiang, Y.Y., Duan, W., Knoblock, C.A.: Extracting human settlement footprint from historical topographic map series using context-based machine learning. In: 8th International Conference of Pattern Recognition Systems. pp. 1–6 (2017)
65. Uhl, J.H., Leyk, S., Chiang, Y.Y., Duan, W., Knoblock, C.A.: Spatialising uncertainty in image segmentation using weakly supervised convolutional neural networks: A case study from historical map processing. IET Image Processing **12**(11), 2084–2091 (2018)
66. Uhl, J.H., Leyk, S., Chiang, Y.Y., Duan, W., Knoblock, C.A.: Automated extraction of human settlement patterns from historical topographic map series using weakly supervised convolutional neural networks. IEEE Access **8**, 6978–6996 (2019)
67. Uhl, J.H., Leyk, S., Chiang, Y.Y., Knoblock, C.A.: Towards the automated large-scale reconstruction of past road networks from historical maps. Computers, Environment and Urban Systems **94**, 101794 (2022)
68. Uhl, J.H., Leyk, S., Li, Z., Duan, W., Shbita, B., Chiang, Y.Y., Knoblock, C.A.: Combining remote-sensing-derived data and historical maps for long-term backcasting of urban extents. Remote Sensing **13**(18), 3672 (2021)
69. Ulloa-Torrealba, Y., Stahlmann, R., Wegmann, M., Koellner, T.: Over 150 years of change: Object-oriented analysis of historical land cover in the main river catchment, Bavaria/Germany. Remote Sensing **12**(24), 4048 (2020)
70. Wong, C.S., Liao, H.M., Tsai, R.T.H., Chang, M.C.: Semi-supervised learning for topographic map analysis over time: A study of bridge segmentation. Scientific Reports **12**(1), 18997 (2022)
71. Wu, S., Heitzler, M., Hurni, L.: Leveraging uncertainty estimation and spatial pyramid pooling for extracting hydrological features from scanned historical topographic maps. GIScience & Remote Sensing **59**(1), 200–214 (2022)
72. Wu, S., Schindler, K., Heitzler, M., Hurni, L.: Domain adaptation in segmenting historical maps: A weakly supervised approach through spatial co-occurrence. ISPRS Journal of Photogrammetry and Remote Sensing **197**, 199–211 (2023)
73. Zhang, Y., Yin, Y., Zimmermann, R., Wang, G., Varadarajan, J., Ng, S.K.: An enhanced GAN model for automatic satellite-to-map image conversion. IEEE Access **8**, 176704–176716 (2020)
74. Zhao, Y., Wang, G., Yang, J., Zhang, L., Qi, X.: Building block extraction from historical maps using deep object attention networks. ISPRS International Journal of Geo-Information **11**(11), 572 (2022)
75. Zhou, Z., Rahman Siddiquee, M.M., Tajbakhsh, N., Liang, J.: UNet++: A nested U-Net architecture for medical image segmentation. In: Deep Learning in Medical Image Analysis and Multimodal Learning for Clinical Decision Support. pp. 3–11 (2018)
76. Zhu, J.Y., Park, T., Isola, P., Efros, A.A.: Unpaired image-to-image translation using cycle-consistent adversarial networks. In: Proceedings of the IEEE International Conference on Computer Vision. pp. 2223–2232 (2017)